



P and S velocity structure of the upper mantle beneath the Transantarctic Mountains, East Antarctic craton, and Ross Sea from travel time tomography

Timothy Watson and Andrew Nyblade

*Department of Geosciences, Pennsylvania State University, University Park, Pennsylvania 16802, USA
(andy@geosc.psu.edu)*

Douglas A. Wiens

Department of Earth and Planetary Sciences, Washington University, Campus Box 1169, 1 Brookings Drive, St. Louis, Missouri 63130, USA

Sridhar Anandakrishnan and Margaret Benoit

Department of Geosciences, Pennsylvania State University, University Park, Pennsylvania 16802, USA

Patrick J. Shore

Department of Earth and Planetary Sciences, Washington University, Campus Box 1169, 1 Brookings Drive, St. Louis, Missouri 63130, USA

Donald Voigt

Department of Geosciences, Pennsylvania State University, University Park, Pennsylvania 16802, USA

John VanDecar

Nature, and Department of Terrestrial Magnetism, Carnegie Institution, 1530 P Street, NW, Washington, D. C. 20005, USA

[1] P and S wave travel times from teleseismic earthquakes recorded by the Transantarctic Mountains Seismic Experiment (TAMSEIS) have been used to tomographically image upper mantle structure beneath portions of the Transantarctic Mountains (TAM), the East Antarctic (EA) craton, and the West Antarctic rift system (WARS) in the vicinity of Ross Island, Antarctica. The TAM form a major tectonic boundary that divides the stable EA craton and the tectonically active WARS. Relative arrival times were determined using a multichannel cross-correlation technique on teleseismic P and S phases from earthquakes with $m_b \geq 5.5$. 3934 P waves were used from 322 events, and 2244 S waves were used from 168 events. Relative travel time residuals were inverted for upper mantle structure using VanDecar's method. The P wave tomography model reveals a low-velocity anomaly in the upper mantle of approximately $\delta V_p = -1$ to -1.5% in the vicinity of Ross Island extending laterally 50 to 100 km beneath the TAM from the coast, placing the contact between regions of fast and slow velocities well inland from the coast beneath the TAM. The magnitude of the low-velocity anomaly in the P wave model appears to diminish beneath the TAM to the north and south of Ross Island. The depth extent of the low-velocity anomaly is not well constrained, but it probably is confined to depths above ~ 200 km. The S wave model, within resolution limits, is consistent with the P wave model. The low-velocity anomaly within the upper mantle can be attributed to a 200–300 K thermal anomaly, consistent with estimates obtained from seismic attenuation

measurements. The presence of a thermal anomaly of this magnitude supports models invoking a thermal buoyancy contribution to flexurally driven TAM uplift, at least in the Ross Island region of the TAM. Because the magnitude of the anomaly to the north and south of Ross Island may diminish, the thermal contribution to the uplift of the TAM could be variable along strike, with the largest contribution in the Ross Island region. The tomography results reveal faster than average velocities beneath East Antarctica, as expected for cratonic upper mantle.

Components: 8379 words, 10 figures.

Keywords: East Antarctica; Transantarctic Mountains; upper mantle.

Index Terms: 7203 Seismology: Body waves; 7218 Seismology: Lithosphere (1236); 7270 Seismology: Tomography (6982, 8180).

Received 31 December 2005; Revised 3 April 2006; Accepted 26 April 2006; Published 20 July 2006.

Watson, T., A. Nyblade, D. A. Wiens, S. Anandakrishnan, M. Benoit, P. J. Shore, D. Voigt, and J. VanDecar (2006), P and S velocity structure of the upper mantle beneath the Transantarctic Mountains, East Antarctic craton, and Ross Sea from travel time tomography, *Geochem. Geophys. Geosyst.*, 7, Q07005, doi:10.1029/2005GC001238.

1. Introduction

[2] In this study, we use P and S wave travel times from teleseismic earthquakes recorded by the Transantarctic Mountains Seismic Experiment (TAMSEIS) to tomographically image upper mantle structure beneath portions of the Transantarctic Mountains (TAM), the East Antarctic (EA) craton, and the West Antarctic rift system (WARS) in the vicinity of Ross Island, Antarctica (Figure 1). The TAM represent a major tectonic boundary that divides the stable EA craton and the tectonically active WARS (Figure 1). The TAM stretch across the length of the continent, and while their origin likely results from interaction between the lithospheric structure of the EA craton and the WARS, there remains uncertainty about the exact mechanism(s) for the uplift of the mountain range. Results from this study provide new constraints on upper mantle structure beneath the TAM, the EA craton and parts of the WARS, and are used together with constraints from other studies to evaluate further uplift models for the TAM and the nature of the lithospheric boundary between the WARS and EA craton.

[3] The paper is structured in 3 parts. In the first section we review the geology of EA, the WARS and the TAM, previous geophysical studies of the region, and uplift models for the TAM. The second section contains a description of the data and methodology used for the body wave tomography. Results from the P and S wave travel time inversions and resolution tests are described in the third section, and in the final section we discuss the

implications of the modeling results for understanding TAM uplift and the nature of the lithospheric boundary between the WARS and EA craton.

2. Background

2.1. Geology and Tectonic History of Antarctica

[4] Antarctica can be divided into three main tectonic regions: the East Antarctic (EA) craton, the West Antarctic Rift System (WARS) and the Transantarctic Mountains (TAM) that separate the EA craton and WARS (Figure 1). Due to the vast extent of the EA ice sheet, little is known about the geologic composition and tectonic history of the EA craton, except around its margins where outcrops are exposed along the coast and in parts of the TAM. Glikson [1982] suggested that the EA craton formed from terrain accretion in the late Archean, Elliot [1975] argued that the final assembly of the craton was not achieved until the Paleoproterozoic, and more recently, Fitzsimons [2003] showed that the Neoproterozoic Pinjarra suture might extend through EA, raising the possibility that craton assembly was not complete until the end of the Precambrian.

[5] The WARS is surrounded by four terrains; Marie Byrd Land, the Antarctic Peninsula, the Ellsworth-Whitmore Mountains, and the Thurston Island block [Anderson, 1999]. Extension within the WARS began in the Jurassic [Dalziel and Lawver, 2001; Grunow et al., 1991; Lawver and

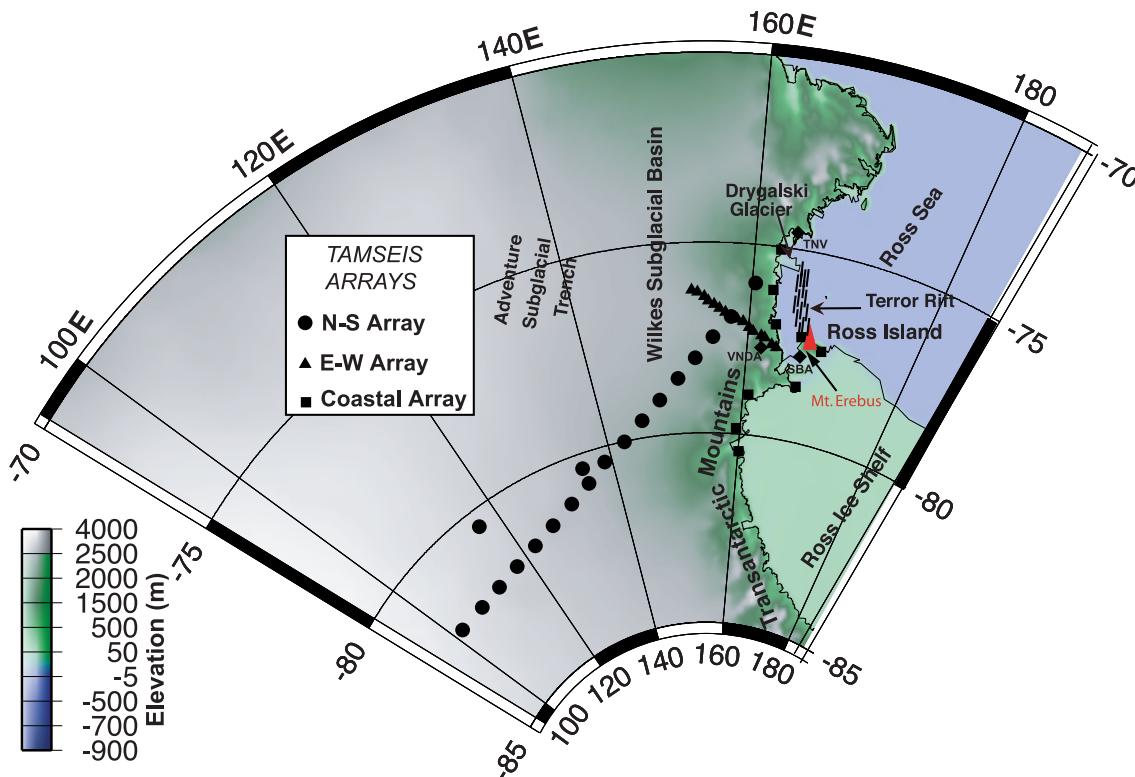


Figure 1. Topographic map showing the location of the Transantarctic Mountains, several other tectonic features relevant to this study, the TAMSEIS seismic stations (arranged in three arrays), and the permanent seismic stations used in this study.

Scotese, 1987; Lawver *et al.*, 1992], and extension is thought to be presently occurring in the Terror rift, a 70 km wide structure 50–100 km east of the TAM front extending through the Western Ross Sea approximately from Mt. Erebus to Mt. Melborne [Cooper *et al.*, 1987] (Figure 1). Active alkaline volcanism is found at the southern end of the Terror rift on Ross Island (Mt. Erebus).

[6] The TAM reach heights of 4500 m and extend approximately 3500 km across the continent, from Northern Victoria Land to the Weddell Sea [Robinson and Splettstoesser, 1984]. The main phase of rock uplift likely began around 55 Ma, with maximum uplift of 5–6 km, as suggested by fission track analysis [Fitzgerald *et al.*, 1986; Fitzgerald, 1992, 1994]. Outcrops throughout the TAM, and especially within the McMurdo Dry Valleys region where the best exposures are found, reveal westward dipping sedimentary strata of the Devonian-Triassic Beacon Supergroup intruded by Jurassic Ferrar dolerite dikes and capped by Kirkpatrick flood basalts [Barrett *et al.*, 1986; Collinson, 1991; ten Brink *et al.*, 1997]. These rocks unconformably overlie the Granite harbor

intrusives and metasediments that are relicts of the Ross Orogeny (500–530 Ma).

2.2. Previous Geophysical Studies

[7] Global- and regional-scale surface wave studies indicate that fast velocities, comparable to other major cratonic regions worldwide, characterize the upper mantle beneath East Antarctica and that the TAM overlie a boundary between the seismically fast upper mantle of the EA craton and the seismically slow upper mantle of the WARS [Sieminski *et al.*, 2003; Danesi and Morelli, 2001; Ritzwoller *et al.*, 2001; Morrelli and Danesi, 2004; Ekstrom *et al.*, 1997; Roult and Rouland, 1994; Montanger and Tanimoto, 1991]. However, the precise location of the boundary is uncertain because the lateral model resolution in these studies is limited. Bannister *et al.* [2000] performed a regional scale surface-wave study utilizing data from the permanent stations SBA, TNV, and VND and found shear wave velocities 6% lower than PREM [Dziewonski and Anderson, 1981] beneath the Terror rift, and 2% lower to the west beneath the TAM front. Lawrence *et al.* [2006a, 2006b] generated phase velocity maps

for fundamental mode Rayleigh waves recorded on the TAMSEIS stations and then inverted the phase velocities jointly with receiver functions for crust and upper mantle structure. The results of the joint inversion revealed a low-velocity anomaly in the upper mantle beneath the coastal region and extending ~ 50 – 150 km inland beneath the TAM front from the coast, at least in the vicinity of Ross Island (Figure 1).

[8] Crustal structure has been investigated in a number of studies. Bentley [1991] reported average crustal thickness of 35–45 km for the EA craton based on surface wave dispersion and seismic refraction analyses. Studinger *et al.* [2003] used receiver functions and gravity measurements near Lake Vostok to obtain an approximate crustal thickness of 35 km. Lawrence *et al.* [2006b], from their joint inversion of receiver functions and Rayleigh wave phase velocities, found an average crustal thickness of 35 ± 2 km across the EA craton. Lawrence *et al.* [2006b] obtained a maximum crustal thickness of 40 ± 2 km beneath the crest of the TAM decreasing to 20 ± 2 km along the coast. Bannister *et al.* [2003] utilized receiver function analysis to demonstrate a change in crustal thickness from 38 ± 2 km about 85 km inland from the coast beneath the TAM to 31 ± 2 km about 10 km inland from the coast. Within the Terror rift region of the WARS, several studies found crust ~ 18 – 25 km thick [Behrendt, 1999; Brancolini *et al.*, 1995; Davey and Cooper, 1987]. Bannister *et al.* [2003] estimated a crustal thickness for the WARS of 20 ± 2 km.

[9] Additional constraints on crustal structure are provided by studies of gravity data. Ferraccioli *et al.* [2001] modeled gravity data acquired by the 1998/1999 International Trans-Antarctic Scientific Expedition (ITASE). Their modeling results show crustal thinning in the TAM hinterland, suggesting that the Wilkes Subglacial Basin and Adventure Subglacial Trench may be of rift origin (Figure 1). Studinger *et al.* [2004] modeled gravity data from the 1999/2000 SOAR program [Blankenship *et al.*, 2001; Holt, 2001; Richter *et al.*, 2001; Studinger *et al.*, 2004] and their models show a small (~ 4 km) crustal root under the TAM.

2.3. TAM Uplift Models

[10] Even though the TAM are widely considered to be an example of rift flank uplift, as they parallel the WARS and lack geologic evidence of compressional tectonics [Fitzgerald *et al.*, 1986; Weissel and Karner, 1989; Stern and ten Brink, 1989; Studinger *et al.*, 2004], there is considerable debate about the timing of and exact mechanism for their uplift.

Fitzgerald *et al.* [1986] suggested strain-related isostatic uplift, where strain was unequally partitioned between the crust and the subcrustal lithosphere during the formation of the Ross Embayment. In their model, they included the possibility of an additional buoyancy contribution from magmatic underplating subsequent to the deposition of the Beacon Supergroup. Stern and ten Brink [1989] suggested that uplift of the TAM was the result of a broad flexure of the ridged EA lithosphere along its rifted edge (i.e., the edge of a broken plate). They suggested that a thermal load under the TAM front, due to lateral heat conduction from the hotter WARS mantle, aided in the uplift. Erosion may have also played a role after the initial phase of uplift [Stern and ten Brink, 1989; ten Brink and Stern, 1992]. ten Brink *et al.* [1997] refined the interpretation of Stern and ten Brink [1989], suggesting that the decoupling of the Antarctic lithosphere between EA and the WARS was not concurrent with the formation of the Ross Embayment in the Cretaceous but instead occurred in response to Paleocene-Eocene (61–53 Ma) trans-tensional plate motion [Cande *et al.*, 1995, 2000].

[11] Recently, a number of other uplift mechanisms have been proposed. Studinger *et al.* [2004] and Karner *et al.* [2005] suggested a model which favors rift flank uplift at ~ 80 Ma enhanced by climate-induced erosional unloading circa 55 Ma. This uplift model does not invoke a thermal anomaly in the lithosphere to aid in the uplift, but does require a crustal root beneath the TAM to provide a source of buoyancy. Stern *et al.* [2005] suggested that the isostatic response due to glacial incision may account for as much as 50% of the peak elevations in some places, arguing that the paleoclimatic conditions were such that the peaks were preserved while the warmer, lower elevations were continually incised, thus producing anomalously large relief between the peaks and valleys. Finally, Lawrence *et al.* [2006b] combined estimates of crustal thickness and upper mantle velocity variation with the SOAR gravity data to address the uplift of the TAM. They proposed a hybrid uplift model invoking isostasy from crustal thickening (~ 5 km), thermal loading, erosional unloading, and a flexural response associated with rift flank uplift.

3. Methods

3.1. TAMSEIS Experiment

[12] This study utilizes data from the Transantarctic Mountains Seismic Experiment (TAMSEIS),

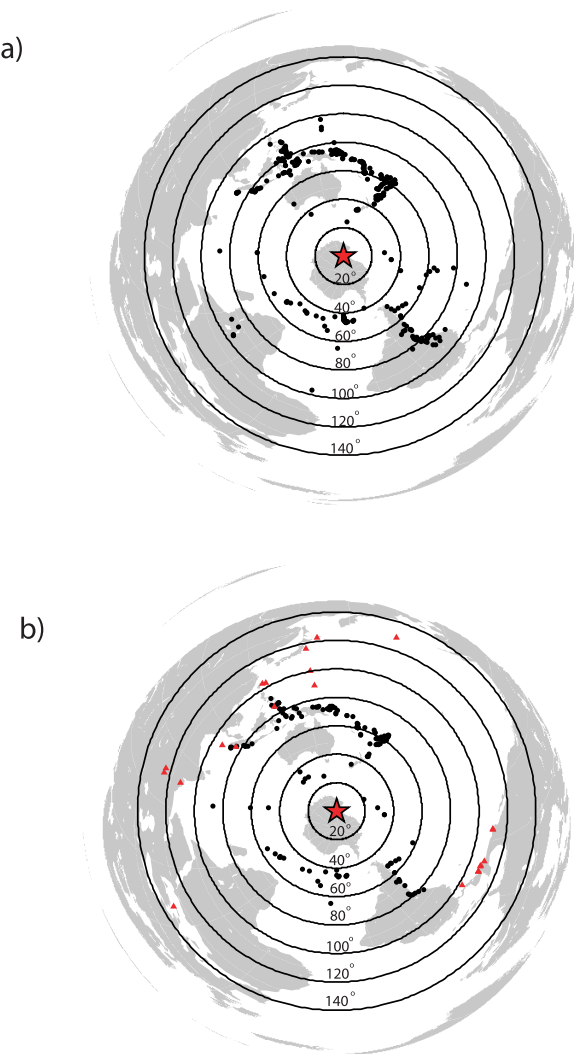


Figure 2. (a) Map of event locations used for P wave travel times (black dots). The red star represents the center of the TAMSEIS experiment, and the concentric rings denote great circles of angular spacing (in degrees) from the center of the experiment. (b) Map of event locations used for S wave travel times. The black dots show the event locations for S waves, and the red triangles show the event locations for SKS waves. The red star represents the center of the TAMSEIS experiment, and the concentric rings denote great circles of angular spacing (in degrees) from the center of the experiment.

which consisted of 42 temporary broadband stations deployed from November 2000 to December, 2003 in three arrays (Figure 1). The first array consisted of 16 stations spaced roughly 20 km apart extending 300 km east-west through the TAM from Mt. Barnes to the eastern edge of the Wilkes Subglacial Basin (E-W Array, Figure 1). The second array consisted of 17 stations spaced

approximately 80 km apart, extending 1400 km from Terra Nova (TNV) NNE-SSW across the TAM onto the East Antarctic craton (N-S Array, Figure 1). The third array consisted of 9 stations spread north-south along the coast and around Ross Island (Coastal Array, Figure 1). In addition to the TAMSEIS stations, data used in this study come from 3 permanent broadband stations of the Global Seismic Network, VNDA, SBA & TNV (Figure 1).

3.2. Relative Arrival Time Determination

[13] Relative arrival times were determined using the multichannel cross-correlation (MCCC) technique of *VanDecar and Crosson* [1990] on teleseismic P and S phases from earthquakes with $m_b \geq 5.5$. P wave picking was performed on vertical component waveforms after applying a 0.1–2.0 Hz band-pass filter. 3934 P waves were picked from 322 events ranging in epicentral distance from approximately 30 to 105 degrees. S waves were picked on the horizontal components after applying a 0.04–0.1 Hz band-pass Butterworth filter. Both the S (picked on the transverse component) and SKS (picked on the radial component) phases were utilized to increase the azimuthal ray coverage, as there were fewer well recorded S waves compared to P waves. In total, 2244 S waves were picked from 168 events ranging in epicentral distance from 30 to 138 degrees. The azimuthal distribution of events is relatively good, as illustrated in Figure 2, with most of the events coming from the subduction zones of the western Pacific and the western coast of South America, and mid-ocean ridges surrounding Antarctica.

[14] The multichannel cross correlation consists of three parts: (1) a cross correlation of all possible trace pairs to find the correlation maxima, (2) a least squares minimization and inversion to minimize errors and find the optimum arrival time on each trace, and (3) calculation of uncertainty estimates of the optimized picks. The cross correlation is performed on a windowed portion of each trace around an initial pick. Window lengths of 3 and 15 seconds were used for the P and S phases, respectively. P travel time residuals ranged from –2.1 to 2.3 sec and S residuals from –4.9 to +5.3 sec.

3.3. Inversion of Travel Time Residuals

[15] The relative arrival time residuals were inverted using the method of *VanDecar* [1991]. The model parameterization consisted of 25 knots (nodes) in latitude between –71 and –87 degrees, 42 knots in longitude between 91E and 179E

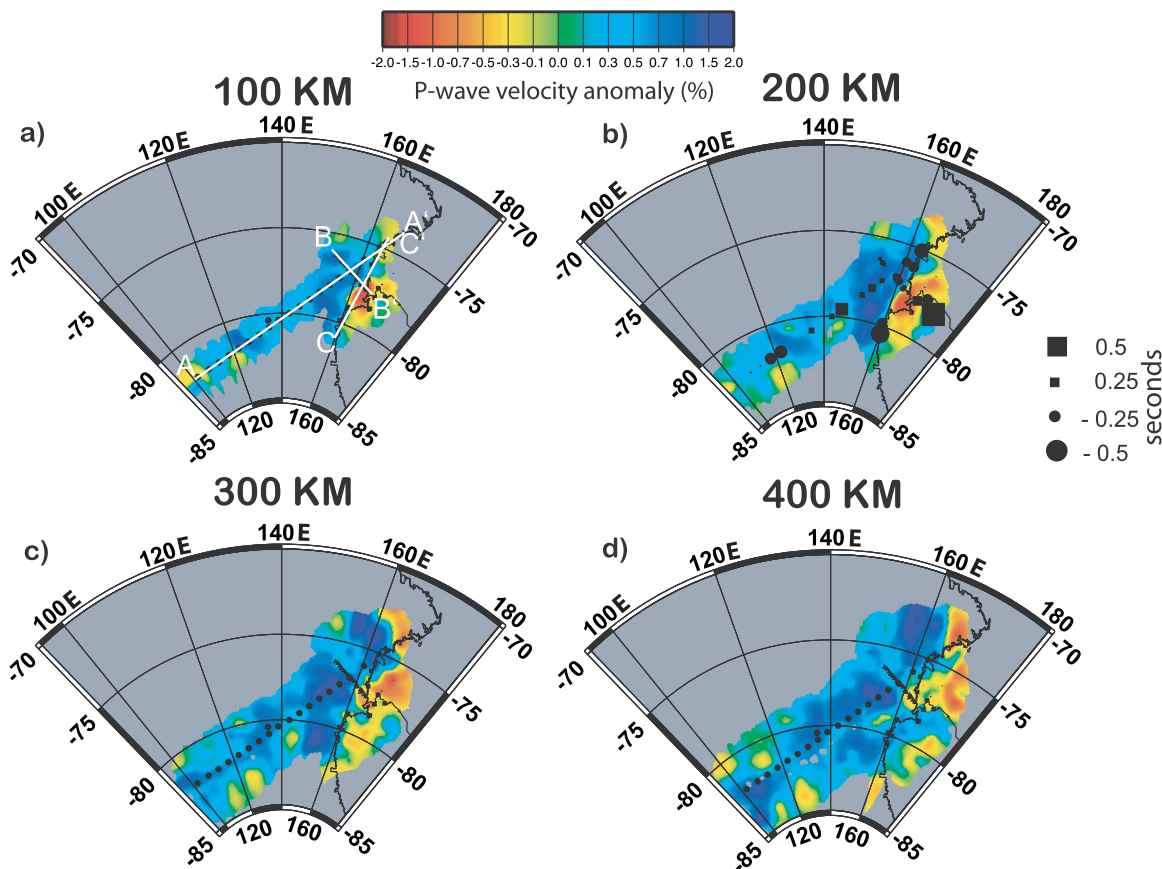


Figure 3. Horizontal slices through the P wave velocity model at depths of 100, 200, 300, and 400 km. Model areas with a hit count of ≥ 15 are shown. Small squares and circles in Figure 3b give station terms. The white lines in Figure 3a denote the locations of transects A-A', B-B', and C-C' in Figure 4.

degrees, and 34 knots in-depth extending from the surface to 1600 km depth, for a total of 35,700 knots. Within the central portion of the model, knots were spatially distributed at intervals of 0.5 degrees in latitude and 2 degrees in longitude. In-depth, knots were spaced 25 km apart in the upper most 200 km of the model, 50 km apart between 200 and 1300 km depth and 100 km apart between 1300 and 1600 km depth.

[16] In the VanDecar method, travel times residuals are simultaneously inverted for slowness perturbations, station corrections and event corrections using an iterative procedure (conjugate gradients). The station corrections absorb near surface residual anomalies resulting from heterogeneous crustal structure (e.g., variations in ice thickness, elevation, crustal structure), while travel time anomalies resulting from event mislocations and heterogeneous structure outside the model domain are mapped into event corrections [VanDecar, 1991]. The starting model for the inversion was the IASP91 model of Kennett and Engdahl [1991].

Optimum smoothing and flattening parameters were selected through an investigation of tradeoff curves. Optimal parameters resulted in a P wave model with a residual reduction of 96% and an S wave model with a residual reduction of 89%.

4. Results

4.1. P Wave Results

[17] Depth slices through the P wave tomography model reveal a low-velocity anomaly in the upper mantle of approximately $\delta V_p = -1$ to -1.5% in the vicinity of Ross Island and extending laterally 50 to 100 km beneath the TAM from the coast (Figure 3). From 100 km to 300 km depth the anomaly trends away from the TAM front to the NNE beneath the Ross Sea (Figure 3). A cross section along transect B-B' (the E-W sub-array, Figure 4b) reveals a sharp boundary on the western edge of the low-velocity anomaly approximately 80 km inland from the coast, placing the contact between regions of fast and slow velocities beneath

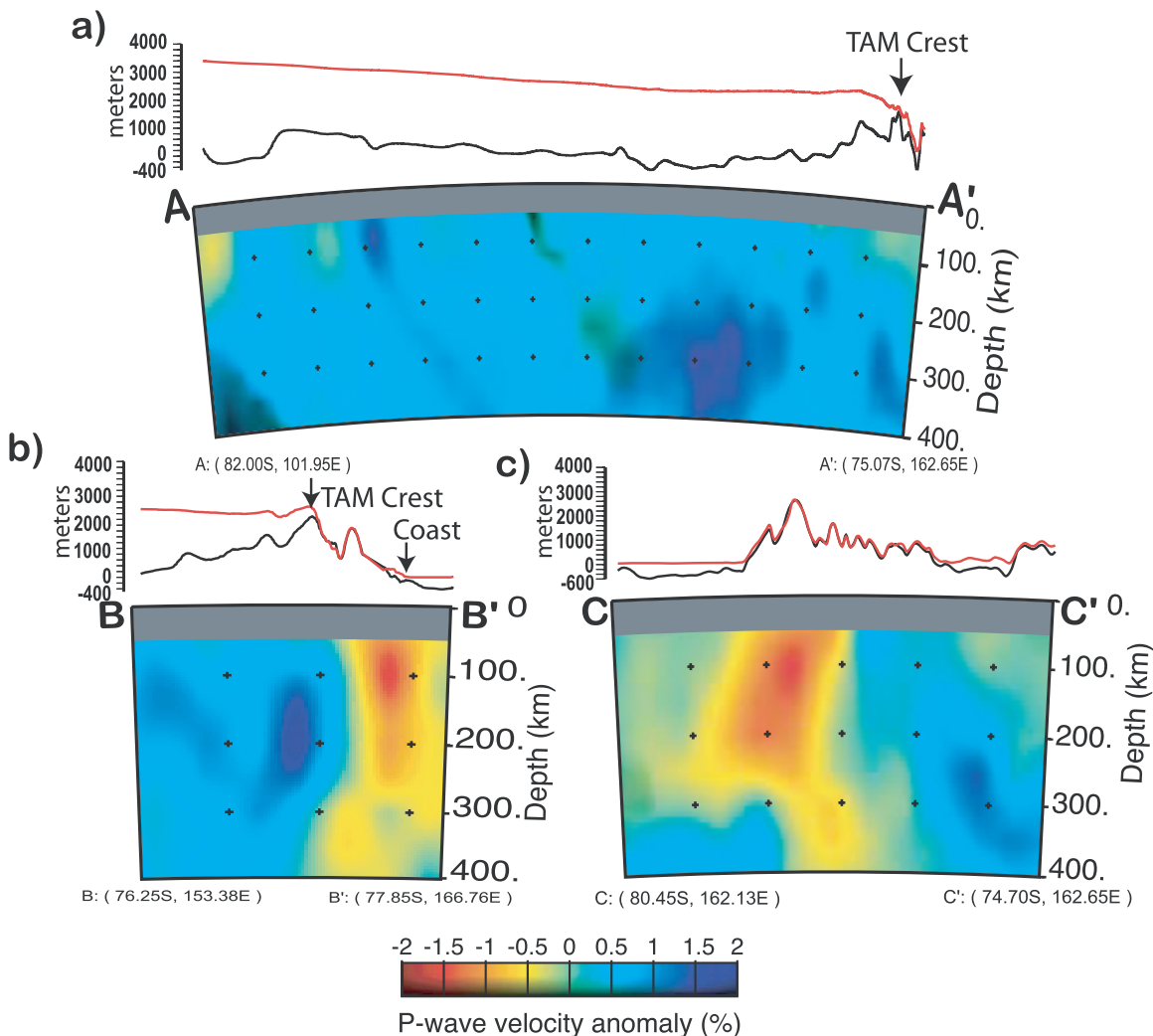


Figure 4. Vertical slices to 400 km depth through the P wave model for transects A-A', B-B', and C-C'. The locations of the transects are shown in Figure 3a. On the top portion of each figure, the red line shows the elevation of the ice sheet and the black line shows the bed elevation [Lythe et al., 2001].

the TAM. The magnitude of the anomaly appears to diminish laterally beneath the TAM to the north and south away from Ross Island, as can be seen in Figure 4c. Overall, the East Antarctic craton is characterized by faster than average velocities ($\delta V_p = 0.5$ to 2%) (Figures 3 and 4), and there is little indication of a low-velocity region within the upper mantle.

4.2. P Wave Resolution Tests

[18] Several tests were conducted to assess model resolution. Synthetic travel time data sets were created for a range of mantle structures, including checkerboards and spikes, and inverted using the same inversion parameters as used in the actual tomography. The checkerboard tests consisted of alternating positive and negative ($\pm 5\%$) spherical

(50 km radius) velocity anomalies, each with a Gaussian fall-off from a specified half-width (Figure 5). Lateral resolution is good (i.e., 50 km diameter spheres can be resolved) beneath most areas of the TAMSEIS network in the 100–400 km depth range. Lateral resolution is also good at 50 km depth under the E-W array where station spacing is smallest.

[19] Vertical resolution is more limited (Figure 6). Vertical smearing along ray paths can be seen beneath all three arrays, indicating that little information is provided in the models about the depth extent of the anomalies. However, the observation that the low-velocity anomaly centered beneath Ross Island does not extend deeper than ~ 300 km (Figure 4) indicates that the low velocity is probably a fairly shallow feature (i.e., the anomaly is probably

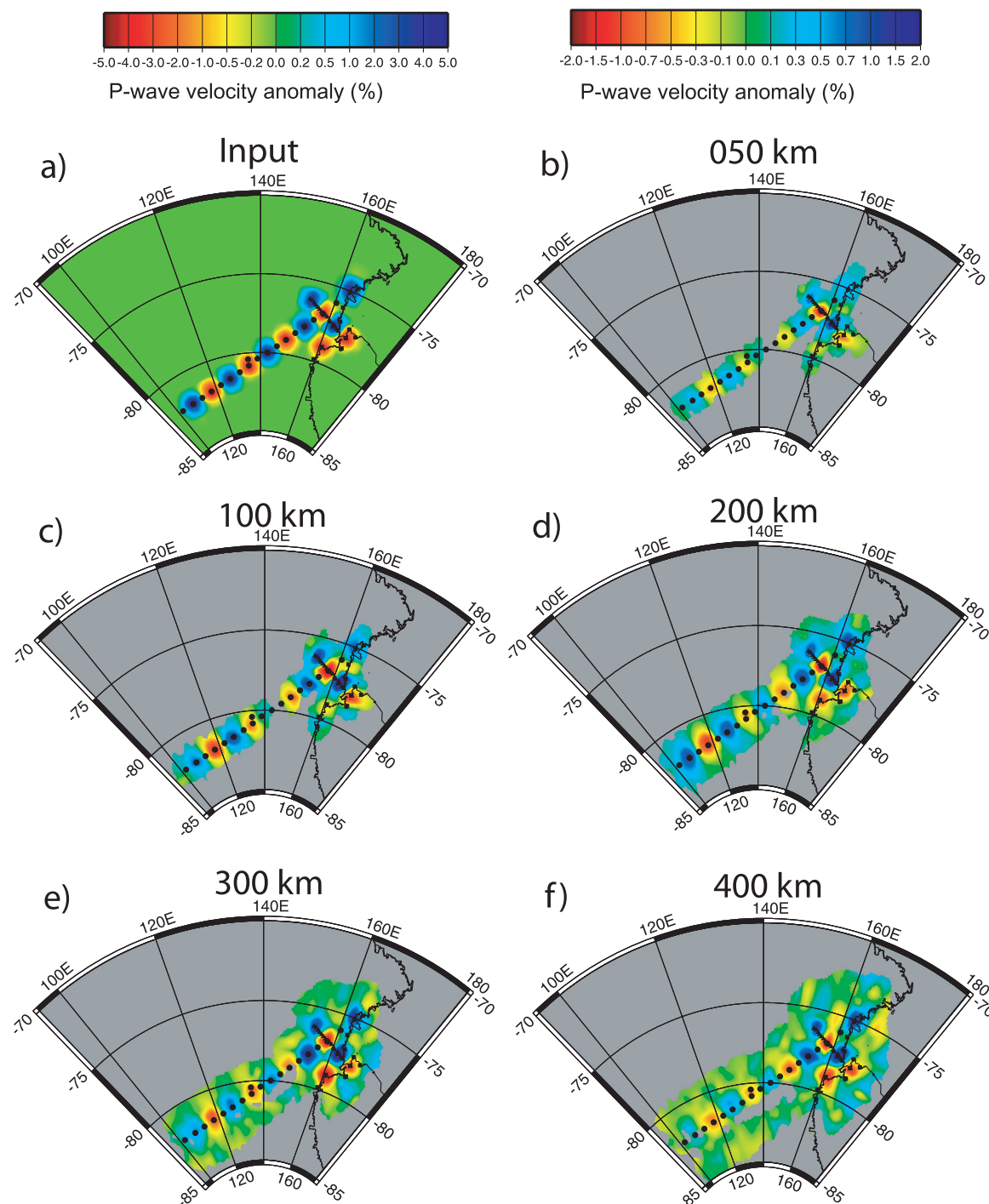


Figure 5. P wave resolution test with alternating $\pm 5\%$ spherical (radius 50 km) slowness anomalies beneath the three arrays. (a) Map displaying input model geometry. (b–f) Results for depth slices at 100, 150, 200, 300 and 400 km. (Note: the input map (Figure 5a) is plotted on a 5% scale, while the other maps (Figures 5b–5f) are plotted on a 2% scale.)

confined to depths above ~ 200 km), and does not exist throughout the entire upper mantle.

[20] Overall, the P wave model appears to recover 40–50% of the initial amplitude anomaly in the

best-resolved portions of the model (i.e., beneath the E-W array and the central portion of the Coastal array). Amplitude recovery and resolution are reduced along the N-S array due to the linear receiver geometry and wider station spacing. Other

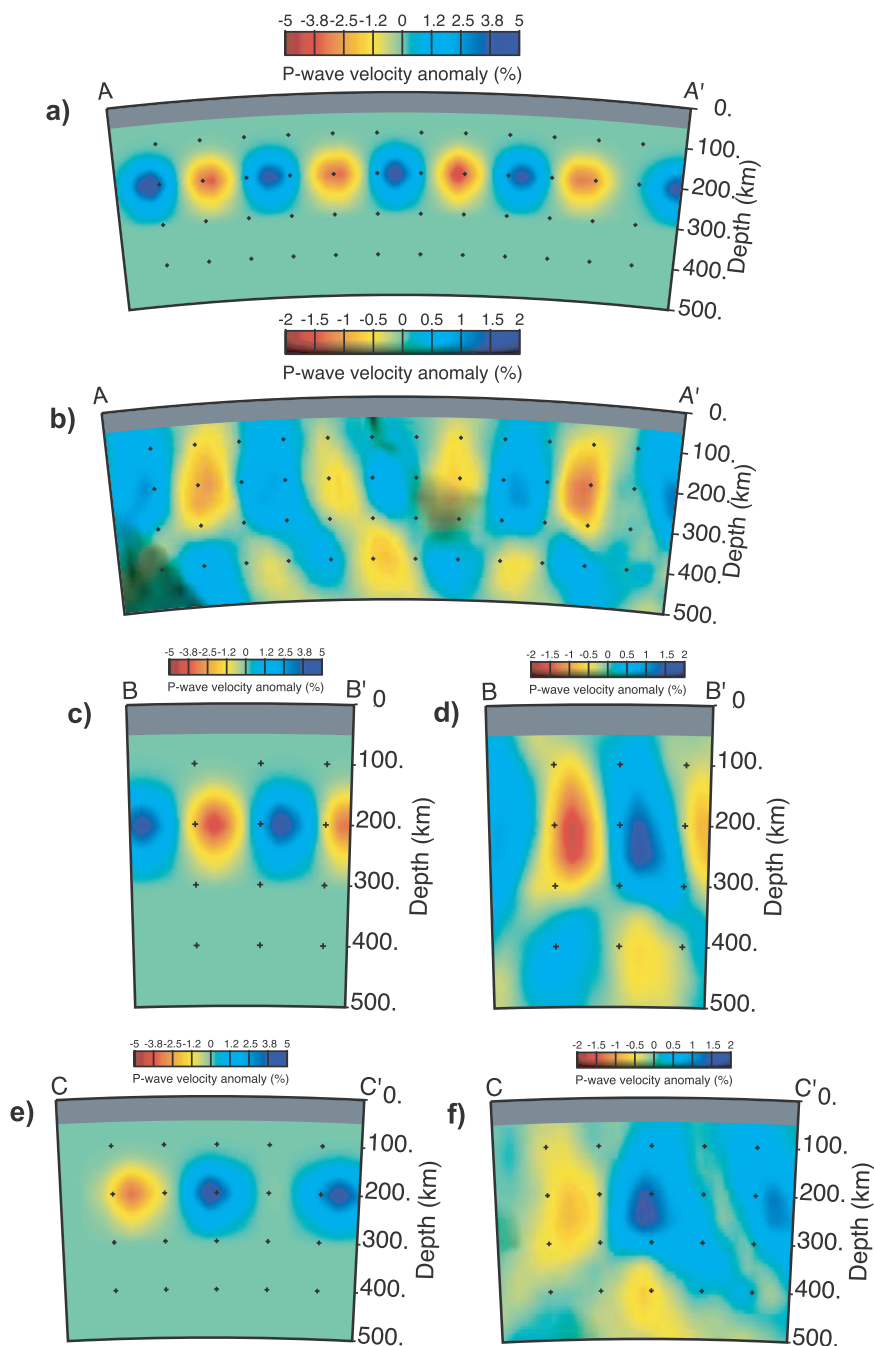


Figure 6. P wave resolution test with alternating $\pm 5\%$ spherical (radius 50 km) slowness anomalies beneath the three arrays centered at 200 km depth. (a, c, e) Cross sections through the input model along transects A-A', B-B', and C-C'. (b, d, f) Cross sections through the resolution test along transects A-A', B-B', and C-C', respectively. (Note: the input map (Figure 6a) is plotted on a 5% scale, while the other maps (Figures 6b–6f) are plotted on a 2% scale.)

studies utilizing VanDecar's method have sighted $<50\%$ amplitude recovery in resolution tests [Wolfe *et al.*, 2002; Bastow *et al.*, 2005; Benoit *et al.*, 2006]. Model results are not displayed for depths deeper than 400 km because resolution rapidly degrades below 400 km depth due to a drop off

in crossing ray paths. Additional resolution tests are described by Watson [2005].

4.3. S Wave Results

[21] Results for the S tomography are similar to the P tomography. Depth slices through the S wave

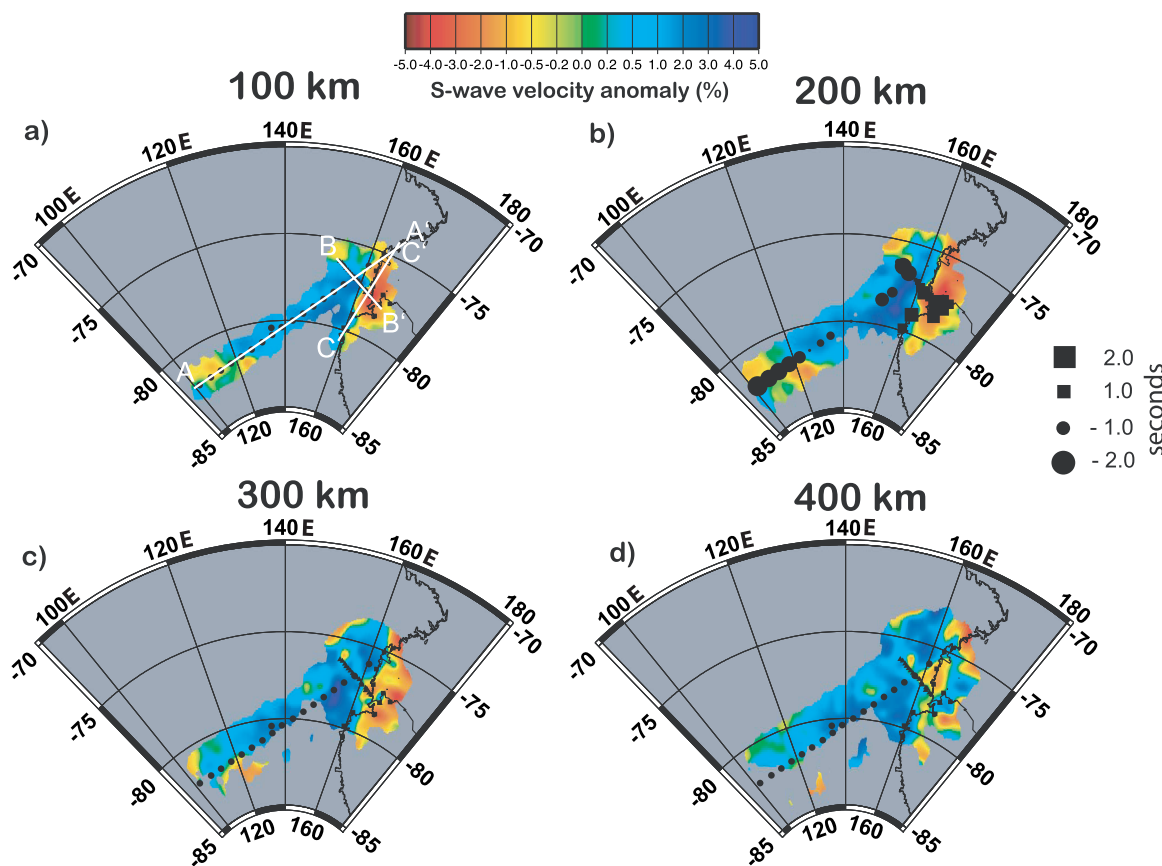


Figure 7. Horizontal slices through the S wave velocity model at depths of 100, 200, 300, and 400 km. Model areas with a hit count of ≥ 15 are shown. Small squares and circles in Figure 7b give station terms. The white lines in Figure 7a denote the locations of transects A-A', B-B', and C-C' in Figure 8.

model reveal a low-velocity anomaly of approximately $\delta V_s = -2.5$ to -4% in the vicinity of Ross Island extending laterally beneath the TAM front from the coast (Figure 7). Cross section B-B' (Figure 8b) shows that this low-velocity anomaly has nearly the same depth extent and sharp boundary under the TAM as the anomaly imaged in the P wave model (Figures 3 and 4), and cross section A-A' (Figure 8a) shows fast cratonic upper mantle ($\delta V_s = 1.2$ to 4%) beneath EA, also consistent with the P-model (Figure 4a). The two models, however, show a major difference in the northward extent of the LVZ beneath the TAM front above ~ 200 km depth. The S wave model shows a continuous low-velocity zone northward and southward along the TAM front and throughout the Ross Sea. The lateral continuity of the low S wave anomaly along the TAM front persists to ~ 200 – 300 km depth.

4.4. S Wave Resolution

[22] Similar to the P wave model, a series of tests were conducted to evaluate the resolution of the S

wave model. Checkerboard tests (Figure 9) indicate good horizontal resolution beneath the E-W array at depths of 50–400 km, but under the coastal and N-S arrays, good lateral resolution is obtained only in the 200–300 km depth range. Vertical resolution is also best under the E-W array, but even there significant smearing along ray paths can be seen (Figure 10). Amplitude recovery is also poorer for the S model than for the P model. In particular, amplitude recovery is poor beneath the northern stations of the Coastal array (Figure 10) where we find a difference in the P and S models (the S model shows a low-velocity anomaly extending under the TAM front whereas the P model does not). However, the total amplitude of the S wave anomaly is similar to TAMSEIS surface wave phase velocity inversion results [Lawrence et al., 2006b], suggesting the actual velocity variations may not be significantly larger than reported here. Overall, the resolution (vertical and horizontal) of the S model is limited compared to the P model, as would be expected because of

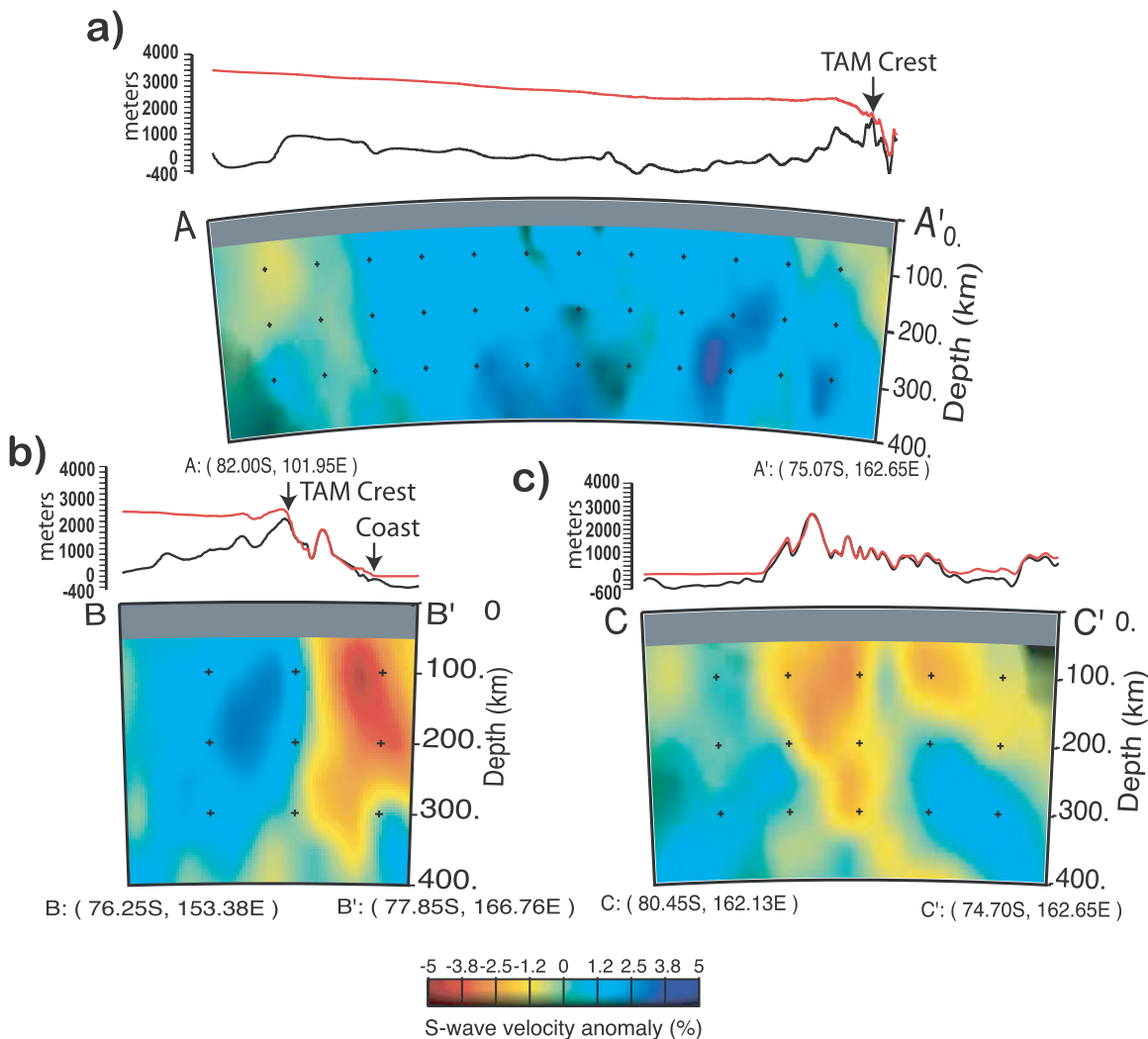


Figure 8. Vertical slices to 400 km depth from the S wave model for transects A-A', B-B', and C-C'. The locations of the transects are shown in Figure 7a. On the top portion of each figure, the red line shows the elevation of the ice sheet, and the black line shows the bed elevation from BEDMAP [Lythe et al., 2001].

the smaller number of travel time residuals used in the inversion.

5. Discussion

[23] The importance of the tomography images presented in this study stems from their superior lateral resolution compared to many other tomographic images of the upper mantle beneath Antarctica [e.g., Morrelli and Danesi, 2004; Ritzwoller et al., 2001; Danesi and Morelli, 2001; Roult and Rouland, 1994]. The images obtained in this study are consistent with global and continental-scale images [e.g., Morrelli and Danesi, 2004; Ritzwoller et al., 2001; Danesi and Morelli, 2001; Roult and Rouland, 1994] in that a major boundary between fast upper mantle under EA and slow upper mantle

under the WARS is seen in the vicinity of the TAM front. However, the images show new details of upper mantle structure along the boundary between the WARS and the EA craton not seen in other studies, in particular, (1) a sharp, vertical boundary between slow and fast velocities in the TAM lithosphere well inland from the coast and (2) a low P wave velocity anomaly in the upper mantle beneath the TAM that is less pronounced to the north and south of Ross Island. In this section, we discuss the tectonic implications of these findings.

5.1. Lateral Extent of Velocity Anomaly Around Ross Island

[24] Both the P and S wave models show similar low-velocity anomalies in the upper mantle ($\delta V_p \sim -1.5\%$, $\delta V_s \sim -3.5\%$ relative to the average

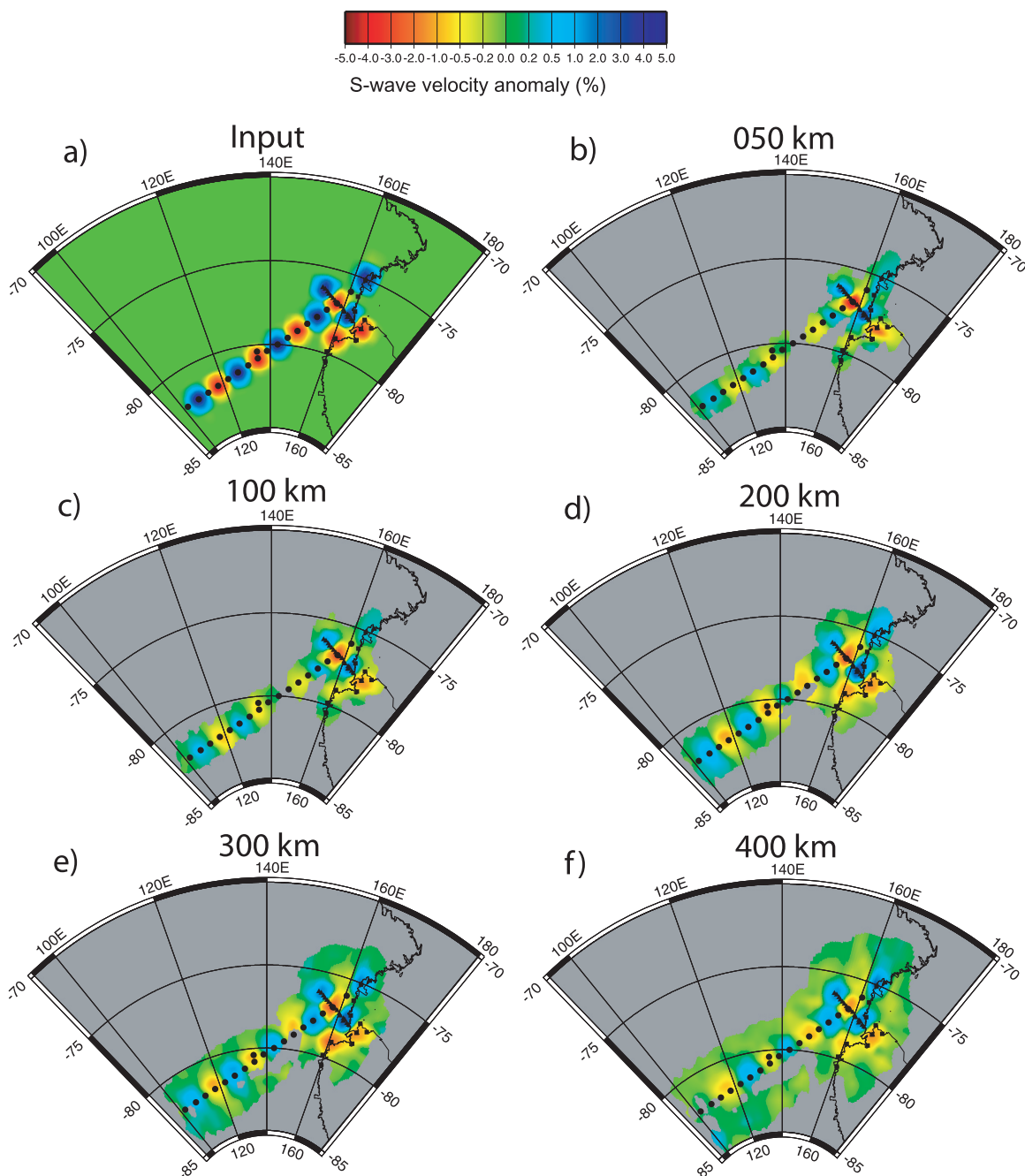


Figure 9. S wave resolution test with alternating $\pm 5\%$ spherical (radius 50 km) slowness anomalies beneath the three arrays. (a) Map displaying input model geometry. (b–f) Results for depth slices at 100, 150, 200, 300, and 400 km.

model) beneath Ross Island and McMurdo Sound that extend westward 50–100 km inland beneath the TAM. The anomaly, as described previously, exhibits a nearly vertical termination, characterized by a 2–3% P velocity change and a 5–6% S velocity change over a distance of ~ 20 –30 km (Figures 3, 4, 7, and 8). The edge of the anomaly is well inland from the coast (Figures 3, 4, 7, and 8), and its position is similar to the edge of the low-

velocity anomaly in the uppermost mantle imaged by Lawrence *et al.* [2006b]. From the P wave model, which has significantly better resolution than the S wave model, it appears that the magnitude of the low-velocity anomaly under the TAM may diminish to the north and south of Ross Island.

[25] At 100 km depth, the P wave model does not show the low-velocity anomaly extending beneath the Terror rift (Figures 3 and 4). But by 200 km

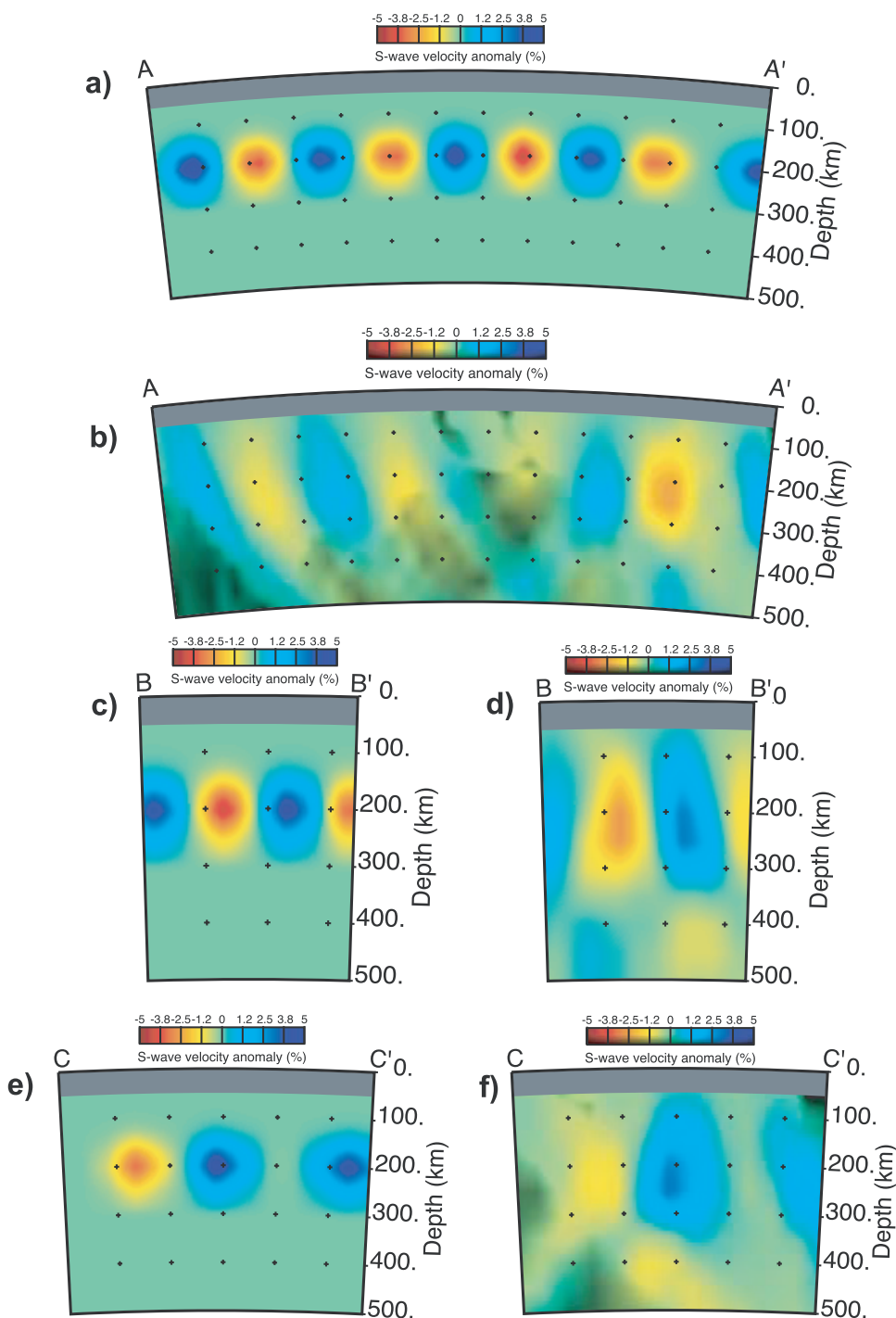


Figure 10. S wave resolution test with alternating $\pm 5\%$ spherical (radius 50 km) slowness anomalies beneath the three arrays centered at 200 km depth. (a, c, e) Cross sections through the input model along transects A-A', B-B', and C-C'. (b, d, f) Cross sections through the resolution test along transects A-A', B-B', and C-C', respectively.

depth, the low-velocity anomaly can be seen beneath its southern edge, and by 300 km depth the low-velocity anomaly appears beneath most of the Ross Sea, with the exception of the coastal area in the vicinity of the Drygalski Ice Tongue. The P wave model probably does not show low velocities

under the Terror rift above ~ 200 km depth because of limited resolution, and our results cannot be used to rule out the existence of shallower low-velocity structure under the Terror rift.

[26] As described previously, the S wave model is somewhat different from the P wave model in that

it shows the low-velocity anomaly extending northward through the western Ross Sea as far north as Northern Victoria land. Resolution tests indicate that the northern portion of the S model is not well resolved. Amplitude recovery is poor and there is pronounced smearing along the ray paths in this part of the S model. The P-model, however, while also subject to smearing along ray paths, recovers the input structure better than the S-model in the western Ross Sea region. Both the P and S wave models show the low-velocity anomaly decreasing in intensity to the south of Ross Island (100–300 km depth), as the anomaly trends offshore to the SSE beneath the Ross Ice Shelf.

[27] In contrast to the region around Ross Island, the P and S models show only minor velocity variations beneath the interior of the EA craton, indicating fairly uniform upper mantle structure not unexpected for cold and thick cratonic lithosphere. The small velocity variations that are observed occur mainly around the edges of the model where the model resolution degrades.

5.2. Thermal Implications of Ross Island Velocity Anomaly

[28] Variations in seismic wave velocity are commonly attributed to temperature variations and chemical heterogeneity. In the upper mantle, effects of temperature tend to dominate over compositional effects [Karato, 1993; Goes *et al.*, 2000; Faul and Jackson, 2005]. Bannister *et al.* [2000] obtained a maximum temperature anomaly of approximately 300 K, using the method of Karato [1993] and assuming that no partial melt is present in the mantle. For their calculation, they used an S velocity anomaly of 0.3 km/s and assumed high attenuation ($Q = 50$). Lawrence *et al.* [2006c] performed a differential attenuation analysis with S wave data and found that the observed Q variation corresponds to upper mantle temperature variations of 200–400 K using relationships from Faul and Jackson [2005].

[29] Here we estimate the upper mantle temperature variations based on our S wave model and the variation of the shear modulus with temperature at seismic frequencies, including the effect of attenuation [Jackson *et al.*, 2002; Faul and Jackson, 2005]. These studies suggest a temperature derivative of about 1.2 m/s/K at an average temperature of 1250°C, for typical upper mantle grain sizes (10 mm). Our observed S wave velocity anomaly of approximately 6% (0.26 km/s) between Ross

Island and EA gives a temperature variation of 210 K. The temperature variation will be somewhat larger if the magnitude of the velocity anomaly is not fully recovered in our S wave model. Thus both velocity and attenuation observations are consistent with a 200–300 K average upper mantle temperature difference between EA and the Ross Island region. A temperature anomaly of 200–300 K, as well as the depth extent of this anomaly suggested by the tomography images of ~200 km, is also similar to the temperature anomaly estimated by *ten Brink and Stern* [1992] using contrasting flexural rigidities across the region. If water is present in the upper mantle beneath the WARS, as suggested by Finn *et al.* [2005], then the size of the temperature anomaly estimated from the velocity variations could be smaller.

5.3. Implications for TAM Uplift

[30] The flexural uplift models for the TAM described in section 2 require a buoyant thermal load in the upper mantle to achieve the uplift and denudation constrained by fission track measurements. In these models, the thermal anomaly results from lateral heating of the thicker lithosphere under the TAM adjacent to thinner lithosphere under the WARS following rifting at ~80 Ma. Our models reveal a low-velocity anomaly in the upper mantle that extends 50–100 km laterally under the TAM front, consistent with thermally modified TAM lithosphere. The temperature anomaly inferred from the seismic anomaly (200–300 K) is sufficient to create the thermal buoyancy load invoked in the uplift models reviewed in section 2.

[31] However, our results suggest that heating of the TAM lithosphere might be variable along the TAM front, as the magnitude of the low-velocity anomaly in the P wave model appears to diminish to the north and south from Ross Island along the TAM front. This result leaves open the possibility that the heating of the TAM lithosphere might be stronger in the Ross Island region compared to elsewhere along the TAM front. If this is the case, then the flexure models of *Stern and ten Brink* [1989] and *ten Brink et al.* [1997] and the hybrid model of Lawrence *et al.* [2006b] could be valid for the Ross Island region but the thermal uplift component in their models might be less important in other parts of the TAM. In these regions, different uplift mechanisms may be important, such as those recently presented by *Studinger et al.* [2004] and *Karner et al.* [2005] invoking a com-

bination of rift flank uplift at circa 80 Ma during the initial development of the WARS followed by isostatic adjustments circa 55 Ma during a period of rapid denudation triggered by climate change.

5.4. Origin of the Thermal Anomaly

[³²] The seismic images in Figures 3, 4, 7, and 8 suggest that there may be a localized thermal anomaly beneath the Ross Island volcanic complex and Terror rift, perhaps superimposed on a broad thermal anomaly associated with the entire WARS, as indicated by continental and global scale tomographic images showing low velocities at upper mantle depths beneath much of the WARS [Morrelli and Danesi, 2004; Ritzwoller *et al.*, 2001; Danesi and Morelli, 2001; Roult and Rouland, 1994]. A localized thermal anomaly could have formed under the Ross Island Volcanic Complex and Terror rift by a plume, as has been previously suggested [e.g., Kyle *et al.*, 1992; Behrendt, 1999]. Indeed, Sieminski *et al.* [2003] find evidence for low seismic velocities beneath Ross Island extending down to the transition zone, possibly suggesting a plume. Alternatively, the thermal anomaly could reflect small-scale convection beneath the Terror rift, similar to the small-scale convection beneath other continental rifts (e.g., Kenya and Baikal) proposed by Slack *et al.* [1994] and Gao *et al.* [2003].

5.5. Implications for the EA Craton Boundary

[³³] The sharp, vertical boundary in the lithosphere under the TAM characterized by a 2–3% P velocity change and a 5–6% S velocity change over a distance of ~20–30 km (Figures 3, 4, 7, and 8) suggests that cold, thick undeformed lithosphere of the EA craton extends beneath the TAM. The position of this boundary is somewhat different than the position inferred from continental-scale tomographic images and satellite-magnetic anomalies [Finn *et al.*, 2006]. Finn *et al.* [2006] suggest, on the basis of a correlation between the area of highest wave speed in the continental-scale tomography images and the satellite-magnetic anomaly pattern, that the boundary between the part of the craton which has not been deformed since the mid Paleoproterozoic and the younger deformed part lies inboard from the TAM (i.e., the boundary does not extend beneath the TAM). The location of this boundary beneath the TAM suggested by the tomographic images in this study illustrates the higher lateral resolution afforded by the TAMSEIS

data set compared to the data sets used in the continental-scale images.

6. Summary

[³⁴] This study utilizes broadband seismic data from the TAMSEIS experiment in a body wave tomography to image upper mantle structure beneath the EA craton, the TAM and the WARS. P and S wave relative arrival times were obtained for teleseismic earthquakes using the MCCC method of VanDecar and Crosson [1990]. Travel time residuals were then inverted using the method of VanDecar [1991] to produce upper mantle P and S wave velocity images. A number of tests were conducted to evaluate the resolution of the P and S wave models. Both models are best resolved in the central portion of the TAMSEIS network (i.e., along the E-W array and central portion of the Coastal array) and resolution toward the edges of the models degrades. The higher ray density of the P model has resulted in better resolution overall than in the S model.

[³⁵] The P and S wave tomography images reveal a low-velocity region, interpreted as a 200–300 K thermal anomaly, within the upper mantle centered beneath Ross Island and extending 50–100 km inland beneath the adjacent McMurdo Dry Valleys portions of the TAM. The strength of the anomaly in the P wave model appears to diminish to the north and south of Ross Island along the TAM front. The presence of the thermal anomaly corroborates models invoking a thermal buoyancy contribution to flexurally driven TAM uplift, at least in the Ross Island region of the TAM. Because the strength of the thermal anomaly may be variable along the TAM front to the north and south of Ross Island, additional buoyancy forces may be important for explaining uplift elsewhere along the mountain range. The tomography results reveal fast velocities beneath East Antarctica as expected for cratonic upper mantle.

Acknowledgments

[³⁶] We would like to thank Tim Stern and Carol Finn for constructive reviews and Mitchell Barklage, Bruce Beaudoin, Jerry Bowling, James Conder, Juliette Florentin, Audrey Huerta, Jesse Lawrence, Bruce Long, Bob Osburn, Tim Parker, John Pollack, Sara Pozgay, Moira Pyle, Brian Shiro, Rigobert Tibi, and many other individuals for assistance in preparing, deploying, and retrieving TAMSEIS stations and data. This work has been funded by the National Science Foundation under grants OPP9909603 and OPP9909648.

References

- Anderson, J. B. (1999), *Antarctic Marine Geology*, 289 pp., Cambridge Univ. Press, New York.
- Bannister, S., R. K. Sneider, and M. L. Passier (2000), Shear-wave velocities under the Transantarctic Mountains and Terror Rift from surface wave inversion, *Geophys. Res. Lett.*, 27, 281–284.
- Bannister, S., J. Yu, B. Leitner, and B. L. N. Kennett (2003), Variations in crustal structure across the transition from West to East Antarctica, Southern Victoria Land, *Geophys. J. Int.*, 155(3), 870–880.
- Barrett, P. J., D. H. Elliot, and J. F. Lindsey (1986), The Beacon Supergroup (Devonian-Triassic) and Ferrar Group (Jurassic) in the Beardmore Glacier area, Antarctica, in *Geology of the Central Transantarctic Mountains, Antarct. Res. Ser.*, vol. 36, edited by M. D. Turner and J. F. Splettstoesser, pp. 339–428, AGU, Washington, D. C.
- Bastow, I. D., G. W. Stuart, J.-M. Kendall, and C. J. Ebinger (2005), Upper mantle seismic structure in a region of incipient continental breakup: Northern Ethiopian rift, *Geophys. J. Int.*, 162(2), 479–493.
- Behrendt, J. C. (1999), Crustal and lithospheric structure of the West Antarctic Rift System from geophysical investigations — A review, *Global Planet. Change*, 23, 25–44.
- Benoit, M. H., A. A. Nyblade, and J. C. VanDecar (2006), Upper mantle P wave speed variations beneath Ethiopia and the origin of the Afar hotspot, *Geology*, 34(5), 329–332, doi:10.1130/G22281.1.
- Bentley, C. R. (1991), Configuration and structure of the subglacial crust, in *The Geology of Antarctica*, edited by R. J. Tingey, pp. 335–364, Clarendon, Oxford.
- Blankenship, D. D., D. L. Morse, C. A. Finn, R. E. Bell, M. E. Peters, S. D. Kempf, S. M. Hodge, M. Studinger, J. C. Behrendt, and J. M. Brozena (2001), Geologic controls on the initiation of rapid basal motion for West Antarctic ice streams: A geophysical perspective including new airborne radar sounding and laser altimetry results, in *The West Antarctic Ice Sheet: Behavior and Environment, Antarct. Res. Ser.*, vol. 77, edited by R. A. Bindschadler, pp. 105–121, AGU, Washington, D. C.
- Brancolini, G., et al. (1995), Seismic stratigraphic atlas of the Ross Sea, Antarctica, in *Geology and Seismic Stratigraphy of the Antarctic Margin, Antarct. Res. Ser.*, vol. 68, edited by A. K. Cooper, P. F. Barker, and G. Brancolini, pp. A271–A286, AGU, Washington, D. C.
- Cande, S. C., C. A. Raymond, J. Stock, and W. F. Haxby (1995), Geophysics of the Pitman Fracture Zone and Pacific-Antarctic plate motion during the Cenozoic, *Science*, 270, 947–953.
- Cande, S. C., J. M. Stock, M. R. D., and T. Ishihara (2000), Cenozoic motion between East and West Antarctica, *Nature*, 404, 145–150.
- Collinson, J. W. (1991), The paleo-Pacific margin as seen from East Antarctica, in *Geological Evolution of Antarctica*, edited by M. R. A. Thompson et al., pp. 199–204, Cambridge Univ. Press, New York.
- Cooper, A. K., F. J. Davey, and J. C. Behrendt (1987), Seismic stratigraphy and structure of the Victoria Land Basin, Western Ross Sea, Antarctica, in *The Antarctic Continental Margin: Geology and Geophysics of the Western Ross Sea*, edited by A. K. Cooper and F. J. Davey, pp. 27–76, Circum-Pacific Counc. for Energy and Nat. Resour., Houston, Tex.
- Dalziel, I. W. D., and L. A. Lawver (2001), Lithospheric setting of the West Antarctic ice sheet, in *The West Antarctic Ice Sheet: Behavior and Environment, Antarct. Res. Ser.*, vol. 77, edited by R. B. Alley and R. A. Bindschadler, pp. 29–44, AGU, Washington, D. C.
- Danesi, S., and A. Morelli (2001), Structure of the upper mantle under the Antarctic Plate from surface wave tomography, *Geophys. Res. Lett.*, 28, 4395–4398.
- Davey, F. J., and A. K. Cooper (1987), Gravity studies of the Victoria Land basin and Iselin Bank, in *The Antarctic Continental Margin: Geology and Geophysics of the Western Ross Sea*, edited by A. K. Cooper and F. J. Davey, pp. 27–76, Circum-Pacific Counc. for Energy and Nat. Resour., Houston, Tex.
- Dziewonski, A. M., and D. L. Anderson (1981), Preliminary reference Earth model, *Phys. Earth Planet. Inter.*, 25, 297–356.
- Ekstrom, G., J. Tromp, and E. W. F. Larson (1997), Measurements and global models of surface wave propagation, *J. Geophys. Res.*, 102, 8137–8157.
- Elliot, D. H. (1975), Gondwana basins of Antarctica, in *Gondwana Geology*, edited by K. S. W. Campbell, pp. 493–536, Aust. Natl. Univ. Press, Canberra, Australia.
- Faul, U. H., and I. Jackson (2005), The seismological signature of temperature and grain size variations in the upper mantle, *Earth Planet. Sci. Lett.*, 234, 119–134.
- Ferraccioli, F., F. Coren, E. Bozzo, C. Zanolla, S. Gandolfi, I. Tabacco, and M. Frezzotti (2001), Rifted (?) crust at the East Antarctic Craton margin: Gravity and magnetic interpretation along a traverse across the Wilkes Subglacial Basin region, *Earth Planet. Sci. Lett.*, 192, 407–421.
- Finn, C. A., R. D. Müller, and K. S. Panter (2005), A Cenozoic diffuse alkaline magmatic province (DAMP) in the southwest Pacific without rift or plume origin, *Geochem. Geophys. Geosyst.*, 6, Q02005, doi:10.1029/2004GC000723.
- Finn, C. A., J. W. Goodge, D. Damaske, and C. M. Fanning (2006), Scouting craton's edge in Paleoproterozoic Gondwana, in *Antarctica—Contributions to Global Earth Sciences (Proceedings of ISAES IX, Potsdam, September 8–12, 2003)*, edited by D. Futterer et al., pp. 165–174, Springer, New York.
- Fitzgerald, P. G. (1992), The Transantarctic Mountains of Southern Victoria Land: The application of fission track analysis to a rift shoulder uplift, *Tectonics*, 11(3), 634–662.
- Fitzgerald, P. G. (1994), Thermochronological constraints on post-Paleozoic tectonic evolution of the central Transantarctic Mountains, Antarctica, *Tectonics*, 13, 818–836.
- Fitzgerald, P. G., M. Sandiford, P. J. Barret, and J. W. Gleadow (1986), Asymmetric extension associated with uplift and subsidence in the Transantarctic Mountains and Ross Embayment, *Earth Planet. Sci. Lett.*, 81(1), 67–78.
- Fitzsimons, I. C. W. (2003), Proterozoic basement provinces of southern and southwestern Australia, and their correlation with Antarctica, in *Proterozoic East Gondwana: Supercontinent Assembly and Breakup*, edited by M. Yoshida, B. F. Windley, and S. Dasgupta, *Geol. Soc. Spec. Publ.*, 206, 93–130.
- Gao, S. S., K. H. Liu, P. M. Davis, P. D. Slack, Y. A. Zorin, V. V. Mordinova, and V. M. Kozhevnikov (2003), Evidence for small-scale mantle convection in the upper mantle beneath the Baikal rift zone, *J. Geophys. Res.*, 108(B4), 2194, doi:10.1029/2002JB002039.
- Goes, S., J. J. Loohuis, M. J. R. Wortel, and R. Govers (2000), The effect of plate stresses and mantle temperatures of northwestern Europe, *Global Planet. Change*, 27, 23–38.
- Grikurov, G. E. (1982), Structure of Antarctica and outline of its evolution, in *Antarctic Geoscience—Symposium on Antarctic Geology and Geophysics, Madison, Wisconsin, August*

- 22–27, 1977, edited by C. Craddock, pp. 791–804, Univ. of Wis. Press, Madison.
- Grunow, A. M., D. V. Kent, and I. W. D. Dalziel (1991), New paleomagnetic data from Thurston Island: Implications for the tectonics of West Antarctica and Weddell Sea opening, *J. Geophys. Res.*, 96, 17,937–17,954.
- Holt, J. W. (2001), Airborne surveys conducted by SOAR for geological studies in Antarctica, 1998–2001, *Eos Trans. AGU*, 82(20), Spring Meet. Suppl., Abstract GP42A-07.
- Jackson, I., J. D. Fitz Gerald, U. H. Faul, and B. H. Tan (2002), Grain-size-sensitive seismic wave attenuation in polycrystalline olivine, *J. Geophys. Res.*, 107(B12), 2360, doi:10.1029/2001JB001225.
- Karato, S. (1993), Importance of anelasticity in the interpretation of seismic tomography, *Geophys. Res. Lett.*, 20, 1623–1626.
- Karner, G. D., M. Studinger, and R. E. Bell (2005), Gravity anomalies of sedimentary basins and their mechanical implications: Application to the Ross Sea basins, West Antarctica, *Earth Planet. Sci. Lett.*, 235, 577–596.
- Kennett, B. L. N., and E. R. Engdahl (1991), traveltimes from global earthquake location and phase identification, *Geophys. J. Int.*, 105, 429–465.
- Kyle, P. R., J. A. Moore, and M. F. Thirlwall (1992), Petrologic evolution of anorthoclase phonolite lavas at Mount Erebus, Ross Island, Antarctica, *J. Petrol.*, 33, 849–875.
- Lawrence, J. F., D. A. Wiens, A. A. Nyblade, S. Anandakrishnan, P. J. Shore, and D. Voigt (2006a), Rayleigh wave phase velocity analysis of the Ross Sea, Transantarctic Mountains, and East Antarctica from a temporary seismograph array, *J. Geophys. Res.*, 111, B06302, doi:10.1029/2005JB003812.
- Lawrence, J. F., D. A. Wiens, A. A. Nyblade, S. Anandakrishnan, P. J. Shore, and D. Voigt (2006b), Crust and upper mantle structure of the Transantarctic Mountains and surrounding regions from receiver functions, surface waves and gravity: Implications for uplift models, *Geochem. Geophys. Geosyst.*, doi:10.1029/2006GC001282, in press.
- Lawrence, J. F., D. A. Wiens, A. A. Nyblade, S. Anandakrishnan, P. J. Shore, and D. Voigt (2006c), Upper mantle thermal variations beneath the Transantarctic Mountains inferred from teleseismic S-wave attenuation, *Geophys. Res. Lett.*, 33, L03303, doi:10.1029/2005GL024516.
- Lawver, L., and C. R. Scotese (1987), A revised reconstruction of Gondwanaland, in *Gondwana Six: Structure, Tectonics and Geophysics*, *Geophys. Monogr. Ser.*, vol. 40, edited by G. D. McKenzie, pp. 17–23, AGU, Washington, D. C.
- Lawver, L. A., L. M. Gahagan, and M. F. Coffin (1992), The development of paleoseaways around Antarctica, in *The Antarctic Paleoenvironment: A Perspective on Global Change, Part I*, *Antarct. Res. Ser.*, vol. 56, edited by J. P. Kennett and D. A. Warnke, pp. 7–30, AGU, Washington, D. C.
- Lythe, M. B., D. G. Vaughan, and the BEDMAP Consortium (2001), BEDMAP: A new ice thickness and subglacial topographic model of Antarctica, *J. Geophys. Res.*, 106(B6), 11,335–11,352.
- Montagner, J. P., and T. Tanimoto (1991), Global upper mantle tomography of seismic velocities and anisotropies, *J. Geophys. Res.*, 96, 20,251–20,337.
- Morrelle, A., and S. Danesi (2004), Seismological imaging of the Antarctic continental lithosphere: A review, *Global Planet. Change*, 42, 155–165.
- Richter, T., J. W. Holt, and D. D. Blankenship (2001), Airborne gravity over East Antarctica, paper presented at KIS 2001: International Symposium on Kinematic Systems in Geodesy, Geomatics and Navigation, Dept. of Geomatics Eng., Univ. of Calgary, Banff, Canada.
- Ritzwoller, M. H., N. M. Shapiro, A. L. Levshin, and G. M. Leahy (2001), Crustal and upper mantle structure beneath Antarctica and surrounding oceans, *J. Geophys. Res.*, 106, 30,645–30,670.
- Robinson, E. S., and J. F. Splettstoesser (1984), Structure of the Transantarctic Mountains determined from geophysical surveys, in *Geology of the Central Transantarctic Mountains, Antarct. Res. Ser.*, vol. 36, edited by M. D. Turner and J. F. Splettstoesser, pp. 119–162, AGU, Washington, D. C.
- Roult, G., and D. Rouland (1994), Antarctica II: Upper mantle structure from velocities and anisotropy, *Phys. Earth Planet. Inter.*, 84, 33–57.
- Sieminski, A., E. Debyle, and J. J. Leveque (2003), Seismic evidence for deep low-velocity anomalies in the transition zone beneath West Antarctica, *Earth Planet. Sci. Lett.*, 216, 645–661.
- Slack, P. D., P. M. Davis, H. A. Dahlheim, A. Glahn, J. R. Ritter, W. V. Green, P. K. H. Maguire, and R. P. Meyer (1994), Crustal and upper mantle structure of the Kenya Rift, *Tectonophysics*, 236, 331–358.
- Stern, T. A., and U. S. ten Brink (1989), Flexural uplift of the Transantarctic Mountains, *J. Geophys. Res.*, 94, 10,315–10,330.
- Stern, T. A., A. K. Baxter, and P. J. Barrett (2005), Isostatic rebound due to glacial erosion within the Transantarctic Mountains, *Geology*, 33, 221–224.
- Studinger, M., G. D. Karner, R. E. Bell, V. Levin, C. A. Raymond, and A. A. Tikku (2003), Geophysical models for the tectonic framework of the Lake Vostok region, East Antarctica, *Earth Planet. Sci. Lett.*, 216, 663–677.
- Studinger, M., R. E. Bell, W. R. Buck, G. D. Karner, and D. D. Blankenship (2004), Sub-ice geology inland of the Transantarctic Mountains in light of new aerogeophysical data, *Earth Planet. Sci. Lett.*, 220, 391–408.
- ten Brink, U. S., and T. A. Stern (1992), Rift flank uplifts and hinterland basins: Comparison of the Transantarctic Mountains with the Great Escarpment of southern Africa, *J. Geophys. Res.*, 97, 569–585.
- ten Brink, U. S., R. I. Hackney, S. Bannister, T. A. Stern, and Y. Makovsky (1997), Uplift of the Transantarctic Mountains and the bedrock beneath the East Antarctic ice sheet, *J. Geophys. Res.*, 102, 27,603–27,621.
- VanDecar, J. C. (1991), Upper-mantle structure of the Cascadia subduction zone from non-linear teleseismic travel time inversion, Ph.D. thesis, Univ. of Wash., Seattle.
- VanDecar, J. C., and R. S. Crosson (1990), Determination of teleseismic relative phase arrival times using multi-channel cross-correlation and least squares, *Bull. Seismol. Soc. Am.*, 80, 150–169.
- Watson, T. D. (2005), The upper mantle structure beneath the Transantarctic Mountains and East Antarctic craton using body wave tomography, M.S. thesis, Penn. State Univ., Univ. Park.
- Weissel, J. K., and G. D. Karner (1989), Flexural uplift of rift flanks due to mechanical unloading of the lithosphere during extension, *J. Geophys. Res.*, 94, 13,919–13,950.
- Wolfe, C. J., S. C. Solomon, P. G. Silver, J. C. VanDecar, and R. M. Russo (2002), Inversion of body-wave delay times for mantle structure beneath the Hawaiian islands: Results from the PELENET experiment, *Earth Planet. Sci. Lett.*, 198, 129–145.